COMMUNICATION

Construction of Streptavidin-based Dual-localized DNAzyme Walker for Disease Biomarker Detection

Received 00th January 20xx,
Accepted 00th January 20xx

DOI: 10.1039/x0xx00000x

Lingying Xia,[a,b] Junbo Chen[b], Xiandeng Hou,[b] Rongxing Zhou[a*], Nansheng Cheng [a*]

A dual-localized DNA walker (dlDW) was constructed by utilizing multiple split DNAzymes with probes, and their substrates are separately localized on streptavidin and AuNPs, serving as walking pedals and tracks, respectively. Upon recognition of the target, the split DNAzymes are self-assembled and activate catalytic activity, enabling rapid walking and signal output. By simply altering the probes, quantitative analysis of protein and nucleic acid disease markers can be achieved in both buffer and serum. This versatile platform shows great potential to be used in clinical disease diagnosis.

DNA nanomachines not only precisely control the structure of DNA on a nanoscale but also manipulate nanoscale mechanical movements for accomplishment of particular tasks.[1, 2] Among various DNA nanomachines, including DNA tweezers,[3-5] DNA scissors,[6] and DNA walkers,[7-10] the three-dimensional (3D) DNA walker is particularly notable for its widespread applications in biosensing and bioimaging.[11, 12] Typically, nanoparticles (e.g., gold nanoparticles, AuNPs) are often used as scaffold for establishment of walking tracks.[13-15] Meanwhile, to enable motion, the walking strands are conjugated onto the same nanosphere, typically powered by DNA strand displacement or enzyme catalysis to drive the operation of DNA walkers. Such co-localized interaction significantly enhances the recognition efficiency between the walking strand and the track strand, thereby greatly improving the walking efficiency. To increase the compactness of operation, DNAzyme is also integrated as a power component on the walking strands, enabling the operation of DNA walkers without the need for protein enzymes.[16-19] Despite the significant advantages demonstrated by these reported DNA walkers, a common drawback in these proposed strategies is the relatively low walking rate that the operational time for current DNA walkers to reach saturation often exceeds one hour.[9, 20] Therefore, the enhancement of walking rate and the decrease of operational time of DNA walkers are highly desired.

To expedite the dynamic operation of DNA walkers, spatial localization of relevant DNA has been proven to be an effective strategy.[21-25] This approach accelerates the associated reactions by increasing the effective concentration of reacting DNAs. For example, introducing multiple DNA substrates onto the walker track surface enables DNAzyme to cyclically walk on the track surface through a well-defined and pre-designed proximity pathway, achieving higher operational rates. Despite some progress in the study of localized DNA walkers, where both the pedal and the track are tethered, their applications are still limited by the slow kinetics of toehold-mediated strand displacement reactions,[26,27] the limited types of target responses,[18,28] and the complex design of nucleic acid sequences.[29,30]

Inspired by previous studies, we herein separately localize the DNA pedal on streptavidin and track nucleic acid on AuNPs, thus achieving dual localization strategy for the construction of DNA walkers. Initially controlled by proteins, four DNA pedals with split 8-17E DNAzymes are designed for assembly, accomplishing the first step of localization and activating DNAzymes. Subsequently, the localized four pedals bind to pre-located substrates on AuNPs. Under the addition of a cofactor, the DNAzyme cyclically cleaves its substrate, facilitating the rapid and efficient operation of the DNA walker. Compared to the localized DNA walkers with different structures, the proposed DNA walker not only significantly enhances the operational efficiency of DNA walkers, but also enables absolute quantification analysis of biomolecules in complex environments. This strategy can potentially provide a pathway for constructing efficient DNA nanodevices, dynamic nanocomputing and DNA-based analytical approaches.

Here, we present a dual-localized DNA walker (dlDW) based on split DNAzymes located on streptavidin, catalyzing

[a] *Division of Biliary Surgery, Department of General Surgery, West China Hospital, Sichuan University, Chengdu, Sichuan 610041, China.*
[b] *Analytical & Testing Center, Sichuan University, Chengdu, Sichuan 610064, China.*
[*] Corresponding authors: zhourongxing@163.com; nanshengcheng@hotmail.com.
Electronic Supplementary Information (ESI) available: [Experimental details, optimization of experimental parameters, dual-localized DNA walker responsive to thrombin in diluted recombinant human serum]. See DOI: 10.1039/x0xx00000x

RNA substrate hydrolysis on AuNPs to construct a controllable and highly effective DNAzyme walker (Scheme 1). The substrates of DNAzymes are functionalized on the surface of AuNPs and served as the moving track, realizing the first-order localization in the DNAzyme walker system (Scheme 1a). Simultaneously, a streptavidin-localized DNA quadrupedal, consisting of four DNAzyme fragments-1 hybridized with four DNAzyme fragments-2 on a streptavidin in the presence of target proteins, is designed to achieve second-order localization (Scheme 1b). In principle, a target protein can be simultaneously recognized by a DNAzyme fragment-1 on the streptavidin-localized DNAzyme fragments-1 and a free-state DNAzyme-2, resulting in the closure of split DNAzyme fragments through binding-induced DNA assembly. Subsequently, the exposed arm segments can hybridize with the substrate on AuNPs. When one of the pedals on streptavidin recognizes a substrate strand on AuNPs, the proximity effect immediately triggers the recognition and catalysis of neighbouring pedals to substrate strands. Furthermore, due to the spatial constraint imposed by streptavidin on the pedals, the pedal structure can consistently be maintained around the AuNPs-DNA track, further facilitating walking efficiency (Scheme 1c). This dual localization strategy involves the efficient recognition and catalysis of surrounding pedals and substrate strands once a pedal on streptavidin identifies a substrate strand on the AuNPs. Such spatial dual-localization imposed by streptavidin ensures the continuous presence of the pedal structure around the DNA-AuNPs track, contributing to the overall enhancement of the DNAzyme walker walking rate.

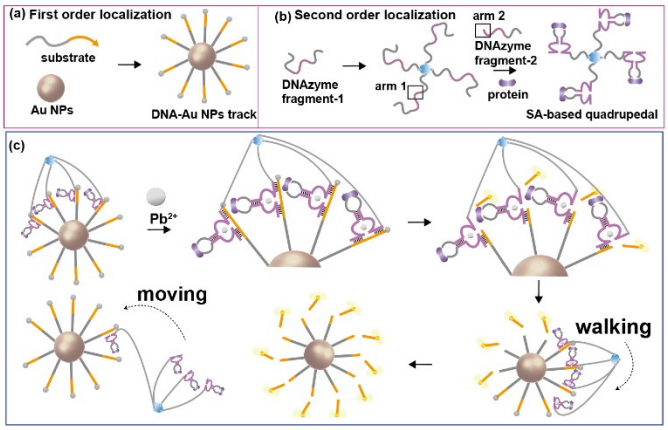

Scheme 1. Schematic illustration of the dlDW. (a) First-order localization process, (b) second order localization process (SA= streptavidin), and (c) the working principle of the constructed DNAzyme walker.

To establish a localized track, a substantial amount of substrates were initially immobilized onto the surface of 20-nanometer AuNPs (Figure S1). The successful functionalization of DNAzyme substrates on the AuNPs was confirmed through ultraviolet-visible absorption spectroscopy (UV-vis) (Figure S2) and potential characterization (Figure S3). For the response signal to remain consistent, the functionalized substrates synthesized on the AuNPs track must demonstrate high reproducibility. Hence, we synthesized functionalized DNA-AuNPs tracks in four batches and quantified the amount of substrate chains on the AuNPs surface for each batch (Figure S4).

To illustrate the superiority of the dual localization of the pedal and track in the constructed DNAzyme walker system, a systematic study was conducted on the reaction kinetics of the constructed DNAzyme walkers. Thus, leveraging the highly stable interaction between streptavidin and biotin, we sequentially designed unipedal, bipedal, tripedal, and quadrupedal DNAzyme walkers based on streptavidin as the carrier, and free unipedal DNAzyme walkers without streptavidin as the carrier (Figure S5). Notably, the pedal and track of the bipedal, tripedal, and quadrupedal walkers based on streptavidin are dual-localized, whereas only the track is single-localized in the unipedal walkers. The pedal of conventional DNA walkers is bound to the track in a 1:1 ratio, while the pedal of DNA dual-localized is bound in a 1:4 ratio. Therefore, the former has a higher chance of escaping from the surface of the AuNPs track, whereas the latter has a lower risk of escape (Figure S6).

To achieve the operation of dlDW, the aptamer for thrombin was incorporated into the two fragments of the split DNAzyme (Figure S7). Consequently, the movement of the DNAzyme walker could be triggered by thrombin. In particular, in the absence of the target thrombin protein, there is no assembly between the two DNAzyme fragments of the walking system, rendering the split DNAzyme in an inactivated state. Upon the introduction of thrombin into the solution, the binding of thrombin to aptamers facilitates the proximity of the two split DNAzyme fragments. Subsequently, each designed walker hybridize with the substrates on the DNA-AuNPs track. In the presence of Pb^{2+}, the split DNAzyme is activated, leading to the cleavage of the substrate and initiating the autonomous and efficient movement of the DNAzyme walker. We monitored the operational efficiency of these DNAzyme walkers individually (Figure 1a and S8a). By real-time fluorescence monitoring, the quadrupedal DNAzyme walker exhibited the highest walking rate (Figure 1b-f). To better understand such difference, the walking rate of each walker was defined and followed the order: quadrupedal DNAzyme walker > tripedal DNAzyme walker > bipedal DNAzyme walker > free unipedal DNAzyme walker > unipedal DNAzyme walker (Figure S8b). To verify such significance, the initial walking rate was then calculated for each of the DNAzyme walkers (Figure S8c) that the rate of the quadrupedal DNAzyme walker is six times higher than the free unipedal DNAzyme walker. It is deduced that the operation of the free unipedal DNAzyme walker relies heavily on the random collision of diffusible DNA fragments, leading to a limited walking rate. In contrast, dual localization allows DNAzyme walkers to have multiple strands that can move simultaneously or sequentially on the track, significantly eliminating the diffusible DNA fragments, therefore exhibiting a significantly increased walking rate.

Additionally, according to the fluorescence kinetics curves, it is evident that before the walking process, each of the various DNAzyme walkers undergoes an assembly process. This signifies the assembly of DNAzyme on the substrate functionalized on the surface of AuNPs. Therefore, the assembly time may also

influence the performance of DNAzyme walkers. To understand whether there is a correlation between localization and the assembly process, the assembly processes of several walkers were compared (Figure S8d). As the number of localized walkers increases, the assembly time gradually decreases, contributing to a shorter assembly time and higher walking efficiency. In contrast, the unipedal DNAzyme walker (non-dual localization) exhibits the longest assembly time, mainly attributed to the absence of the proximity effect in its assembly process. Thus, dual localization contribute the assembly and walking processes for the high efficiency of DNAzyme walkers.

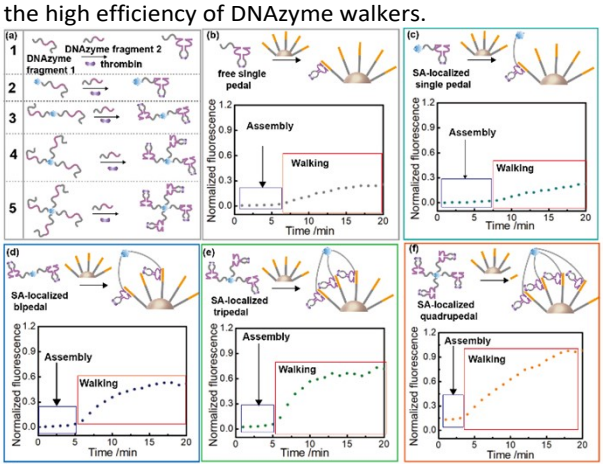

Figure 1. (a) Preparation of various pedals. (b-f) are the fluorescence kinetic curve of free unipedal DNAzyme walker (1), streptavidin-localized unipedal DNAzyme walker (2), streptavidin-localized bipedal DNAzyme walker (3), streptavidin-localized tripedal DNAzyme walker (4) and streptavidin-localized quadrupedal DNAzyme walker (5).

The proposed DNAzyme walker achieves motion through the interaction of localized split DNAzyme with substrates on the AuNP surface. To achieve optimal operational efficiency, relevant parameters were investigated and optimized. Initially, streptavidin was employed as a scaffold for the localization of DNAzyme fragment-1. DNAzyme fragment-2, in a free state, assembles with localization fragment-1 under external stimuli, forming a complex and activating split DNAzyme. Therefore, the ratio between fragment-1 and fragment-2 is crucial. Considering the different triggering mechanisms for protein and nucleic acid-induced assembly, we separately examined the performance of DNAzyme walkers triggered by these two substances at different concentrations of fragment-1 and fragment-2. It was found that at a ratio of 1:40 and 1:10, DNAzyme walkers triggered by both protein and nucleic acid achieved optimal efficiency (Figure S9 and S10).

Meanwhile, the assembled DNAzyme is primarily influenced by Pb^{2+} and substrate concentration. Therefore, these two parameters were optimized separately and found that 2 mM (Figure S12a) and 0.5 mM (Figure S11a) of Pb^{2+}, along with a DNA-AuNPs track concentration of 0.1 nM, were the optimal concentrations. To achieve higher operational efficiency of the walker, we then optimized the loading amount of substrate strands on AuNPs. By preparing two types of AuNP tracks with different densities, a higher amount of substrates (approximately 330 substrates on per AuNP) achieved a faster walking rate compared to a lower amount of substrates (approximately 180 substrates on per AuNP) (Figure S13). Given the physiological environment of DNAzymes and the potential for nonspecific adsorption on AuNPs, we investigated various buffer solutions and pH levels. PBS (Figure S14a) and Tris-HAc (Figure S15a) were found to be the most suitable buffers for the thrombin-triggered DNAzyme walker and microRNA21-triggered DNAzyme walker, respectively. A pH of 8.2 was identified as the optimal choice for both (Figure S12b and Figure S15b).

To evaluate the applicability of the dual localization strategy, nucleic acids were utilized as triggers to examine the functionality of the quadrupedal DNAzyme walker (Figure 2a). We initially attempted to directly induce the assembly of split DNAzyme in the quadrupedal DNAzyme walker using microRNA-21 but observed unobviously increased fluorescent signals (Figure S16). It was speculated that the short length of microRNA-21 might lead to the instability of the quadrupedal DNAzyme walker. Therefore, we employed a structure-switching strategy induced by microRNA-21, employing a longer hairpin structure to trigger the operation of the DNAzyme walker (Figure 2b and c). It was found that the response curve of the DNAzyme walker based on microRNA-21 was similar to that of thrombin. However, the fluorescence kinetics monitoring indicated that the microRNA-21-induced dlDW clearly took longer assembly time than that of the protein-induced dlDW (Figure 2e). This difference may be attributed to the fact that microRNA does not directly hybridize with the two separated DNA segments of split DNAzyme. In such case, before binding to the two separated DNA fragments, the hairpin structure needs to be opened by microRNA-21, subsequently triggering the assembly and operation of the quadrupedal DNAzyme walker.

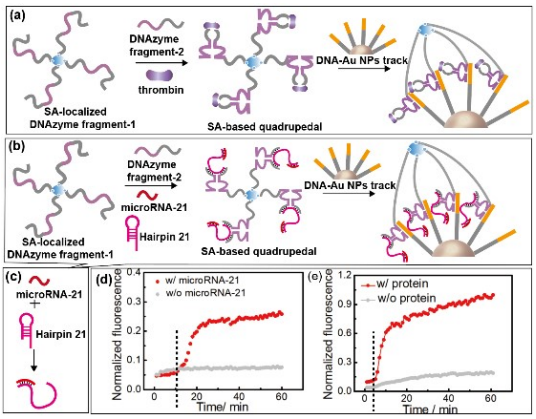

Figure 2. Scheme illustration of the DNAzyme walker assembly process triggered by (a) thrombin and (b) microRNA-21, (c) the recognition of microRNA-21 by Hairpin 21, (d) and (e) are the assembly time corresponding to microRNA-21 and protein as trigger, respectively. SA = streptavidin.

To assess the potential applications of the developed dual localized DNAzyme walker, two detection platforms were designed for quantitation of thrombin and microRNA-21, respectively. As depicted in Figure S17a and d, fluorescence kinetic curves were proportional to various concentrations of thrombin and microRNA-21, suggesting the operation of DNAzyme walker can respond to thrombin and microRNA-21 within the concentration range of 1 pM to 10 nM and 50 pM to 50 nM, respectively. Meanwhile, the corresponding linear range indicate the constructed DNAzyme walker is capable of

achieving quantitative determination of thrombin and microRNA-21 (Figure S17b and e). Furthermore, based on the acceptable stability of DNA-AuNPs tracks in recombinant human serum (Figure S18) and different concentrations of Pb^{2+} (Figure S19), the constructed biosensing platform achieved the quantitative analysis of thrombin in 5% recombinant human serum (Figure S20), and obtained a recovery rate of 98-120% (Table S2), which further underscores its potential for practical sample detection.

Moreover, to investigate the detection specificity of the designed strategy for thrombin, various biomolecules were utilized as interferences against the target thrombin. As depicted in Figure S17c, very weak fluorescence signals were observed with the incubation of 10 nM interferences. However, a robust fluorescence signal was detected in the presence of 1 nM thrombin. Subsequently, the DNAzyme walker was employed to discriminate the mismatched variants of microRNA-21 and wild type of microRNA-21. Owing to different binding affinities, the mismatched variants pose a challenge to triggering the DNA walker operation (Figure S17f). Consequently, the proposed DNAzyme walker demonstrates application potential for both proteins and nucleic acids.

A dual-localized DNAzyme walker (dlDW) was successfully engineered by localizing walking pedals on streptavidin, utilizing assembled split DNAzyme to catalyse localized substrates for fast movement on AuNPs surface. The local concentration was increased between DNAzyme and its substrates, significantly enhancing the reaction kinetics. As a result, the dlDW demonstrated efficiently autonomous movement on AuNPs, accomplishing operation less than one hour. Meanwhile, compared with the traditional DNAzyme walker, the dlDW also shortened the assembly process between the walker and the substrate track, contributing to the accelerated operation of the dlDW. The dlDW can be used for quantitative detection of protein and nucleic acid in simple buffer or biological matrices by altering affinity ligands. Our findings offer valuable insights into designing high-speed DNA walkers, enabling sensitive biomolecule detection and effective biological function regulation.

The authors gratefully acknowledge the financial support for this work from the National Natural Science Foundation of China (22004088, 21705113), Science & Technology Department of Sichuan Province of China (No. 2022NSFSC0650, 2023YFS0183).

Author Contributions

Lingying Xia: Experimental data acquisition, collation, visualization and writing - original draft preparation. Junbo Chen: writing - reviewing and editing, and funding acquisition. Xiandeng Hou: writing - reviewing and editing. Rongxing Zhou and Nansheng Cheng: conceptualization, writing - reviewing and editing, and funding acquisition.

Conflicts of interest

There are no conflicts to declare

Notes and references

1. K. Lund, A. J. Manzo, N. Dabby, N. Michelotti, A. Johnson-Buck, J. Nangreave, S. Taylor, R. Pei, M. N. Stojanovic, N. G. Walter, E. Winfree and H. Yan, *Nature*, 2010, **465**, 206-210.
2. J. Bath, A. J. Turberfield, *Nat. Nanotechnol.,* 2007, 2, 275-284.
3. M. Liu, J. Fu, C. Hejesen, Y. Yang, N. W. Woodbury, K. Gothelf, Y. Liu and H. Yan, *Nat. Commun.*, 2013, **4**, 2127.
4. B. Kou, Y. Chai, Y. Yuan, R. Yuan, *Anal. Chem.*, 2018, **90**, 10701-10706.
5. X. Xu, L. Wang, K. Li, Q. Huang and W. Jiang, *Anal. Chem.*, 2018, **90**, 3521-3530.
6. L. Peng, Y. Yuan, X. Fu, A. Fu, P. Zhang, Y. Chai, X. Gan, R. Yuan, *Anal. Chem.*, 2019, **91**, 3239-3245.
7. G. A. Wang, C. Kong and F. Li, *Chem. Commun.*, 2023, **59**, 5492-5501.
8. K. Chen, Q. Huang, T. Fu, G. Ke, Z. Zhao, X. Zhang and W. Tan, *Anal. Chem.*, 2020, **92**, 7404-7408.
9. S. D. Mason, G. A. Wang, P. Yang, Y. Li and F. Li, *ACS Nano*, 2019, **13**, 8106-8113.
10. B. Yurke, A. J. Turberfield, A. P. Mills Jr, F. C. Simmel & J. L. Neumann, *Nature* 2000, 406, 605-608.
11. X. Yang, Y. Tang, S. D. Mason, J. Chen and F. Li, *ACS Nano*, 2016, **10**, 2324-2330.
12. O. I. Wilner, I. Willner, *Chem. Rev.*, 2012, **112**, 2528-2556.
13. M. Oishi, K. Saito, *ACS Nano*, 2020, **14**, 3477-3489.
14. Z. Yang, X. Peng, P. Yang, Y. Zhuo, Y. Q. Chai, W. Liang, R. Yuan, *Chem. Sci.*, 2020, **11**, 8482-8488.
15. C. Jung, P. B. Allen, A. D. Ellington, *Nat. Nanotechnol.*, 2015, **11**, 157-163.
16. J. Tao, H. Zhang, M. Weinfeld and X. C. Le, *Anal. Chem.*, 2023, **95**, 14990-14997
17. C. Liu, Y. Hu, Q. Pan, J. Yi, J. Zhang, M. He, M. He, T. Chen, X. Chu, *Biosens. Bioelectron.*, 2019, **136**, 31-37.
18. M. Du, J. Zheng, S. Tian, Y. Liu, Z. Zheng, H. Wang, J. Xia, X. Ji and Z. He, *Anal. Chem.*, 2021, **93**, 5606-5611.
19. X. Zhang, X. Wei, J. Qi, J. Shen, J. Xu, G. Gong, Y. Wei, J. Yang, Q. Zhu, T. Bai, Z. Guo, X. Qu, Y. Zhu, *Anal. Chem.*, 2022, **94**, 4787-4793.
20. M. M. Lv, J. W. Liu, R. Q. Yu and J. H. Jiang, *Chem. Sci.e*, 2020, **11**, 10361-10366.
21. Z. Huang, X. Ma, F. Jiang, R. Wang, Z. Wu and Y. Lu, *Nano Letters*, 2023, **23**, 6042-6049.
22. R. Zhou, C. Hu, Y. Jin, J. Zhang, H. Du, P. Yang, J. Chen, X. Hou, N. Cheng, *Anal. Chem.*, 2020, **92**, 8909-8916.
23. H. Bui, S. Shah, R. Mokhtar, T. Song, S. Garg, J. Reif, *ACS Nano*, 2018, **12**, 1146-1155.
24. G. Chatterjee, N. Dalchau, R. A. Muscat, A. Phillips and G. Seelig, *Nat. Nanotechnol.*, 2017, **12**, 920-927.
25. M. Teichmann, E. Kopperger, F. C. Simmel, *ACS Nano* 2014, **8**, 8487-8496.
26. Z. M. Huang, X. B. Ma, F. Jiang, R. Wang, Z. Wu, Y. Lu, *Nano Lett.*, 2023, **23**, 6042-6049.
27. L. Wang, P. Liu, Z. Liu, K. Zhao, S. Ye, G. Liang, J. J. Zhu, *ACS Sens.*, 2020, **5**, 3584-3590.
28. D. Yao, S. Bhadra, E. Xiong, H. Liang, A. D. Ellington, C. Jung, *ACS Nano*, 2020, **14**, 4007-4013.
29. X. M. Zhou, Y. Zhuo, T. T. Tu, R. Yuan, Y. Q. Chai, *Anal. Chem.*, 2022, **94**, 8732-8739.
30. R. X. Zhou, C. J. Hu, Y. W. Jin, J. Zhang, H. Du, P. Yang, J. B. Chen, X. D. Hou, N. S. Cheng, *Anal. Chem.*, 2020, **92**, 8909-8916.

